Spring 7-1-2017

Synthesis of Au/Ag, Pd/Ag and Pt/Ag Nanoparticles by Galvanic Replacement Reaction

Sunnith Kumar Admala
Governors State University

Synthesis of Au/Ag, Pd/Ag and Pt/Ag Nanoparticles by Galvanic Replacement Reaction

A Project Submitted to:

Governors State University

By: Sunnith Kumar Admala

In partial fulfillment of the requirement for the Master of Analytical Chemistry

May 2017

Governors State University

University Park, Illinois

This paper is dedicated to my professors, parents, family, friends, and to all of those who supported me through my academic journey.

Acknowledgements

I would first like to thank my research project advisor Dr. K.G. Sanjaya Ranmohotti. The door to his office was always open whenever I ran into a trouble spot or had a question about my research or writing. He consistently allowed this paper to be my own work and steered me in the right direction whenever he thought I needed it.

I express deepest gratitude to Dr. John Sowa, Dr. Walter Henne, Dr. Joong-Won Shin, and Dr. Shelly Kumar for their assistance and direction throughout my graduate work.

I extend my gratitude to Janith Wazio and Catherine Taffora who guided and helped me to perform my duties as a Graduate Assistant. I would like to thank all the other professors of Chemistry department, to whom I was fortunate in helping them as a Graduate Assistant.

I would also like to acknowledge Dr. Indika U. Arachchige, Assistant Professor at Virginia Commonwealth University, for helping my research work by providing the required data for the samples obtained in research work.

Finally, I express my very profound gratitude to my mother, sister and friends at each level of education, providing me with unfailing support and continuous encouragement throughout my years of study and through the process of researching and writing this thesis.

Table of Contents

List of Figures

Abstract

In recent years, galvanic replacement reactions have been successfully employed to produce bimetallic nanoparticles of a range of shapes, yet to date very few efforts have been devoted to develop methods for synthesizing smaller (<10nm) M/Ag; M=Au, Pt, Pd alloy particles using Ag hollow particles as sacrificial template. In this research work, we investigated new approach for the controllable synthesis of Au/Ag, Pd/Ag, and Pt/Ag alloy nanoparticles by applying galvanic replacement reaction on hollow Ag template in the presence of gold, palladium, and platinum salts. According to TEM analysis, the sizes of Au/Ag, Pd/Ag, and Pt/Ag alloy particle are 7.0±1.6 nm, 6.0±1.2 nm, and 3.0±0.8 nm, respectively. According to the study of optical property measurements on Ag hollow samples with increasing Au, Pt, and Pd content, it was observed that surface plasmon resonance peaks of the Au/Ag particles prepared with higher concentrated $HAuCl_4$ solutions absorb at longer wavelengths and are red-shifted compared to the surface plasmon resonance of Ag hollow template. In the case of adding K_2PdCl_4 to Ag hollow sample resulted in blue shift of surface Plasmon resonance peaks for initial addition of palladium salt and further addition of K_2PdCl_4 caused the Plasmon peaks to diminish. Interestingly, our attempt to make Pt/Ag particle by reacting Ag hollow particles with various amounts of K_2PtCl_4 revealed that resulting alloy particles could still exhibit surface Plasmon resonance peaks for higher Pt content. Usually Pt and Pd nanoparticles do not exhibit surface plasmon resonance peaks in the visible spectrum. This work provides a model for a design of M/Ag; M=Au, Pt, Pd alloy particles, where combining Ag hollow samples with increasing amounts of Au, Pt, and Pd can provide successful execution of tenability of surface plasmon resonance.

Introduction

The synthesis of hollow bimetallic nanoparticles is of interest because of their special, tunable optical properties. Over the last decade there has been intense research focus on the anisotopic noble metal nanoparticles due to their unique optical properties such as localized surface plasmon resonance (LSPR). Nanoparticles are the particles in the size range of 1 to 100 nm. Metallic nanoparticles are different from their bulk metals in consideration to the physical and chemical properties, which were proved to attract various industrial applications. Of the various properties, the optical property is one of the fundamental attractions and a characteristic of a nanoparticle due to its uniqueness.[1] For instance, gold nanoparticles have a characteristic wine red color. Silver nanoparticles are yellowish gray. Platinum and palladium nanoparticles are black in color.

Surface Plasmon Resonance:

The optical properties of noble metal particles originate from localized surface plasmon resonance (LSPR).[2] Surface plasmon of a metal can be explained as a collective oscillation of electrons in the conduction band and they dominate the electromagnetic responses of the metallic structure of dimensions on the order of the plasmon resonance wavelength. The surface plasmon is displayed when electromagnetic field interacts with conduction band electrons and induces the coherent oscillation of electrons. As a result, a strong absorption band appears in some region of the electromagnetic spectrum. A large enhancement of local electric field at a very close proximity to the nanoparticle surface was observed as a result of the surface plasmon resonance (SPR). The metal nanoparticle spectral position is controlled by size, shape, aspect ratio and composition, but if the metal nanoparticle is hollow its spectral position can be controlled by adjusting the wall thickness without making many changes to the nanoparticle size, shape and aspect ratio. The

hollow cavity in a nanoparticle adds a possibility of encapsulation and transport of molecules and materials of interest.

Noble metal-based bimetallic nanoparticles

The bimetallic nanoparticles show better electronic, optical, catalytic or photolytic properties compared to the monometallic nanoparticles. The synergy between the two metals present in a nanoparticle enables it to display new properties in addition to the properties combined from both the noble metals. These properties are assumed to be a result of the structural and electronic effects of the bimetallic structures. Optical, electronic, and catalytic properties depend on the composition of the nanomaterials as well as their structure.[2-5] The orientation of a bimetallic nanoparticle occurs as a random alloy, alloying with an intermetallic compound, and a core-shell structure or cluster-in-cluster structure.[6-7] The orientation of the nanoparticle structure greatly depends on the relative strengths of metal-metal bond, surface energies of bulk elements, relative atomic sizes, preparation method and conditions. This is why the synthesis of nanomaterials such as bimetallic nanostructures is so important. The acutely controlled structures and compositions make it very important to obtain such materials with these properties.[8] Previous experiments have reported that surface plasmon resonance peaks of hollow bimetallic Au/Ag nanostructures are able to be manipulated by controlling the Ag and Au ratio in the replacement reaction used.[9] There have been fewer attempts in studying the optical properties of Pt or Pd based nanometallic and bimetallic nanoparticles. One reason why there are fewer attempts is because Pt and Pd nanoparticles usually do not exhibit surface plasmon resonance peaks in the visible spectrum.[10]

Kirkendall effect

The Kirkendall effect is a classical phenomenon in metallurgy. It refers to a nonreciprocal mutual diffusion process through an interface of two metals so that vacancy diffusion occurs to compensate for the unequality of the material flow and that the initial interface moves.[11-12] The first experiment was performed by Kirkendall in 1942 and the result was confirmed in a replicated experiment in 1947. Aldinger was the first person to pursue an interest in the hollowing of silver nanoparticles caused by the Kirkendall effect.[13] It has been known for more than half a century that porosity may result from differential solid-state diffusion rates of the reactants in an alloying or oxidation reaction. Smigctkas and Kirkendall reported the movement of the interface between a diffusion couple, i.e., copper and zinc in brass, as the result of the different diffusion rates of these two species at an elevated temperature. The Kirkendall effect, was the first experimental proof that atomic diffusion occurs through vacancy exchange and not by the direct interchange of atoms. The net directional flow of matter is balanced by an opposite flow of vacancies, which can condense into pores at dislocations. The Kirkendall experiment established that diffusion of substitutional lattice atoms involves defects that facilitate atomic jumps. In most metals and metallic alloys, as well as most other materials, these atomic defects are empty lattice sites, termed vacancies. Condensation of excess vacancies can give rise to void formation near the original interface and within the fast-diffusion side. These voids are usually explained by outward transport of fast-moving cations through the oxide layer and a balancing inward flow of vacancies to the vicinity of the metal-oxide interface. The pores produced at a metal-metal diffusion couple or near the metal-oxide interface of a growing oxide do not yield monodisperse, ordered arrays but instead form a very heterogeneous ensemble. The observed volume fraction for pores is also commonly much smaller than would be expected for the known material flows.[12] These observations are a

direct result of the large volume of material that vacancies can diffuse into and the large number of defects with which they can react.

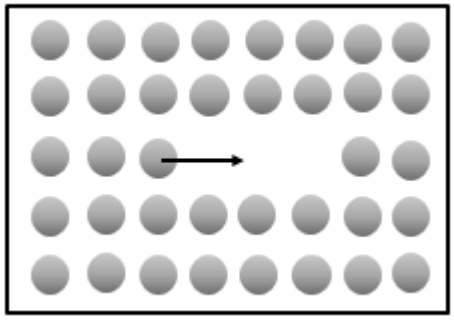

Figure 1: Schematic representation of the vacancy mechanism of atomic diffusions.

Galvanic Replacement Reaction

In recent years, galvanic replacement reactions have been employed to produce bimetallic hollow nanoparticles of a range of shapes. The galvanic replacement reaction is a process in which the metal of higher redox potential is deposited onto a template nanoparticle of material with a lower redox potential.[2] The difference in redox potentials drives the oxidation of the template material by the metal salt precursor of the metal being reduced, resulting in a hollow nanoparticle.[14-18] The most common example is the formation of hollow Au/Ag nanostructures by epitaxial deposition of Au on the edges and faces of a Ag nanoparticle template. This proceeds by reduction of $AuCl_4^-$ alloying of the deposited Au with the underlying Ag, and oxidation of the remaining Ag nanoparticle template, leaving an almost fully enclosed hollow nanostructure. In addition, Pt and Pd containing hollow nanostructures can also be prepared by this approach. Researchers have used this approach to produce a range of enclosed Au/Ag nanoparticles such as cubic nanoboxes,

nanocages, cylindrical nanotubes, spherical nanoshells, and even multiwalled hollow nanostructures.[19-25]

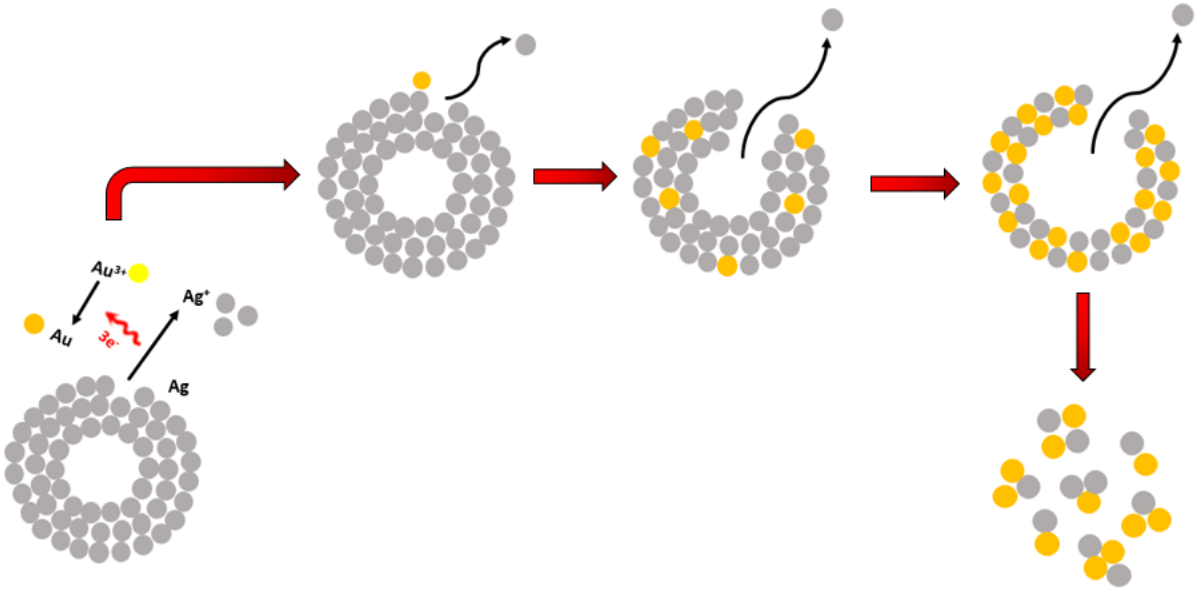

Figure 2: Schematic illustration of the structural evolution at different stages of the galvanic replacement reaction between Ag hollow particle and $HAuCl_4$ in an aqueous solution.

The galvanic replacement reaction includes two stages. At the initial stage, the replacement reaction starts at specific sites with relatively high surface energies and then sea mLess hollow nanostructures with smooth Au−Ag alloy walls were evolved through an integration of galvanic replacement with alloying. Ag atoms also simultaneously migrate into the Au shell to form a sea mLess, hollow nanostructure with Au−Ag alloy wall.[8] This mechanism for galvanic replacement is applicable irrespective of the morphology and composition of the sacrificial templates as long as the presence of appropriate reduction potentials difference between the two metals involved. The reaction conditions of galvanic replacement can be modified so that deposition of metal occurs only on the edges and corners of the template nanoparticle. In this research work, we investigated

new approach for the controllable synthesis of Au/Ag, Pd/Ag, and Pt/Ag alloy nanoparticles by applying galvanic replacement reaction on hollow Ag template in the presence of gold, palladium, and platinum salts.

Experimental Section

Materials:

The $AgNO_3$ (99.9%) ACS grade and L-glutathione reduced (98%) were purchased from Alfa Aesar; $NaBH_4$ (99%) was purchased from Fluka Analytical; NaOH (97%) was purchased from VWR scientific. The metal salts K_2PtCl_4 (99.9%), K_2PdCl_4 (98%), and $HAuCl_4$ (99.99%) were purchased from Sigma-Aldrich. The water used in all the synthesis was 18MΩ Milli-Q filtered.

Synthesis of Ag Hollow Nanoparticles:

The very first step is to synthesize the Ag hollow nanoparticles. The Ag hollow nanoparticles were synthesis by using a literature synthetic method[26] with several modifications. 50 mL of Purified water was taken in a 250 mL round bottomed flask and kept in a freezer until water turned to ice. Once the ice was formed the flask was taken out and set on a magnetic stirrer. Then 3 mL of $AgNO_3$ (10 mM) was added to the ice-cold water followed by the addition of 0.3 mL of L-Glutathione (10 mM) by stirring at a medium speed. After ~4 min, the speed of the stirring (Denville scientific inc, hotplate stirrer) was set to maximum and 10 mL of NaOH (0.1 M) was added by injecting 1 mL aliquot, for 10 times using a micropipette. After the solution turned to pale yellow by vigorous stirring, 3.6 mL of freshly prepared $NaBH_4$ was injected at once into the solution and it was allowed to stir for about ~3-5 min until the color change is stable.

Synthesis of Au/Ag, Pt/Ag and Pd/Ag Hollow Nanoparticles:

Au/Ag alloy hollow particles were synthesized using the Galvanic Replacement Reaction method. The prepared silver hollow nanoparticles solution (66.9 mL) was used in further steps of synthesis. To the above said solution, 20 mL of ascorbic acid (0.3 M) was added while stirring the solution. A solution of 1800µL of 0.1M $HAuCl_4$ in 58.2 mL water was prepared. The $HAuCl_4$ solution (60 mL) was added to the resulting solution at a speed of 1 mL/min using a syringe pump (HSW Norm-Ject). The solution was allowed to stir vigorously and the UV-Visible reading was taken after every 10 mL addition of $HAuCl_4$ solution. The solution was stirred until a stable dark color solution was observed. Similarly, Pt/Ag and Pd/Ag alloy nanoparticles were synthesized using the same sequence of steps as used for synthesis of Au/Ag hollow particles. The $HAuCl_4$ wass replaced with 0.1 M K_2PtCl_4 and 0.1M K_2PdCl_4 for the preparation of Pt/Ag and Pd/Ag alloy particles, respectively.

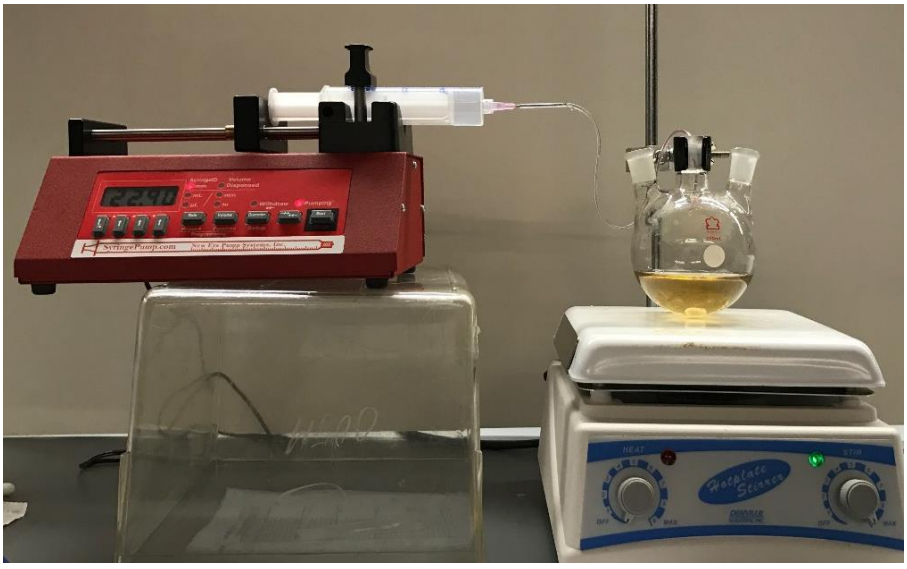

Figure 3: Photograph showing a programmable syringe pump used to add small amounts of solution of $HAuCl_4$, K_2PtCl_4, and K_2PdCl_4 at a given rate.

Characterization

Spectroscopic Instrumentation and Methods:

A PerkinElmer Lamda 35 UV-Vis spectrophotometer was used for optical absorption measurements on Ag hollow nanoparticles and Au/Ag, Pt/Ag, Pd/Ag alloy nanoparticles. The absorption spectrum of the Ag hollow nanoparticles was taken without any dilution whereas the Au/Ag, Pt/Ag and Pd/Ag hollow nanoparticles were diluted 1:3 using purified water. The measurements were taken in the range of 1000 to 300 nm (0.68 eV ~ 6.2 eV).

Powder X-Ray Diffraction (PXRD):

The diffractometer was calibrated using a silicon standard. X-ray powder diffraction data were recorded on a Philips X'Pert system equipped with a Cu K-alpha radiation (l = 1.5418 Å). The powder sample was deposited on a glass slide for XRD measurements. X-ray diffraction patterns were identified by comparison to the phases in X'Pert Highscore Plus along with the ICDD/JCPDS diffraction pattern library. For the particle size calculation, the most intense peak at 38.5° for Au/Ag, 39.75° and 46.1° for Pd/Ag, 39.8° and 46.0° for Pt/Ag were used in the Scherrer calculations.[27]

Transmission Electron Microscopy (TEM):

The TEM equipment used was equipped with JOEL JEM-1230 analytical electron microscope with Gatan Ultrascan 4000SP 4K*4K CCD camera, Leica EM UC6/EM FC6 cryo-ultramicrotome, LKB 2128 ultramicrotome, three LKB Knifemakers, and Ladd vacuum evaporators. The TEM analysis was performed by using JOEL JEM-1230 analytical electron microscope with Gatan

Ultrascan 4000SP 4K*4K CCD camera operating at a 120 kV acceleration voltage. One drop of each Au/Ag, Pt/Ag and Pd/Ag hollow nanoparticles solution was added onto a carbon-coated copper TEM grid and the solvent was allowed to evaporate few hours before introduction to the instrument.

Results and Discussion

The preparation hollow silver nanoparticles alloyed with Au, Pt and Pd starts with the first step of preparation of silver oxide nanoparticles by precipitating silver ions using glutathione as a capping agent in a highly basic solution containing sodium hydroxide. The second step of the preparation is alloying the silver nanoparticles obtained in the above step with Au, Pt, and Pd salts to produce Ag/Au, Ag/Pt and Ag/Pd nanoparticles, respectively.

The preparation involving the first step began with trials using small volumes of the required solutions. The Table 1 shows the amounts of the materials used in the initials trials of preparation of Ag nanoparticles. Figure 4.1 shows the UV-Vis absorbance peak for samples from trial 1 through trial 6 scanned from 700 to 300 nm. Most of the samples were found to have peak position in the range of 460 nm to 490 nm. Figure 4.2 shows peak positions at 531 nm and 474 nm which corresponds to the samples obtained from trial 7 and trial 8, respectively. Based on the observations obtained from the above performed trials and comparing it with the literature, an optimal range of the materials required to prepare the large samples of Ag nanoparticles was setup. The large samples were prepared using more quantities of the materials compared to that of the initial trial batches performed.

Table 1: The amount of materials taken for running the trials 1 through 8 to prepare Ag hollow nanoparticles

Trial #	Purified Water (mL)	10mM $AgNO_3$ (µL)	10mM Glutathione (µL)	0.1M NaOH (µL)	10mM $NaBH_4$ (µL)
1	2.6	150	18	500	180
2	2.6	150	35	500	180
3	2.6	300	60	500	180
4	2.6	300	75	500	180
5	2.6	500	100	500	180
6	2.6	500	150	500	180
7	25	350	25	5000	1800
8	25	1500	180	5000	1800

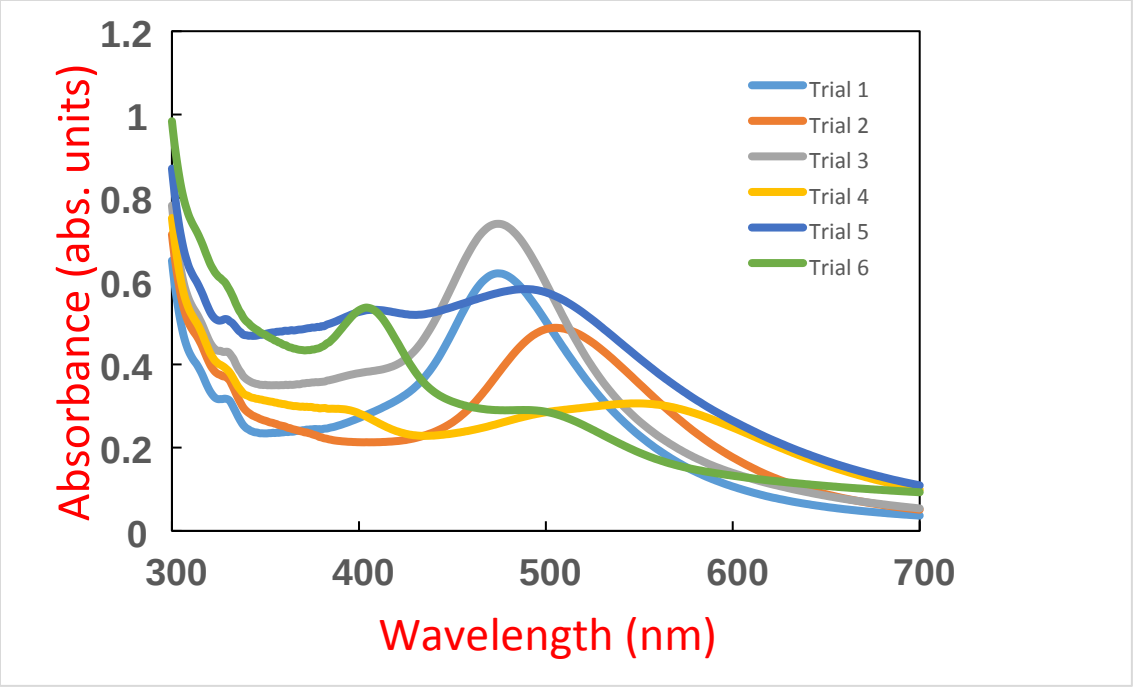

Figure 4.1: The UV-Vis absorbance peak for samples from trial 1 through trial 6.

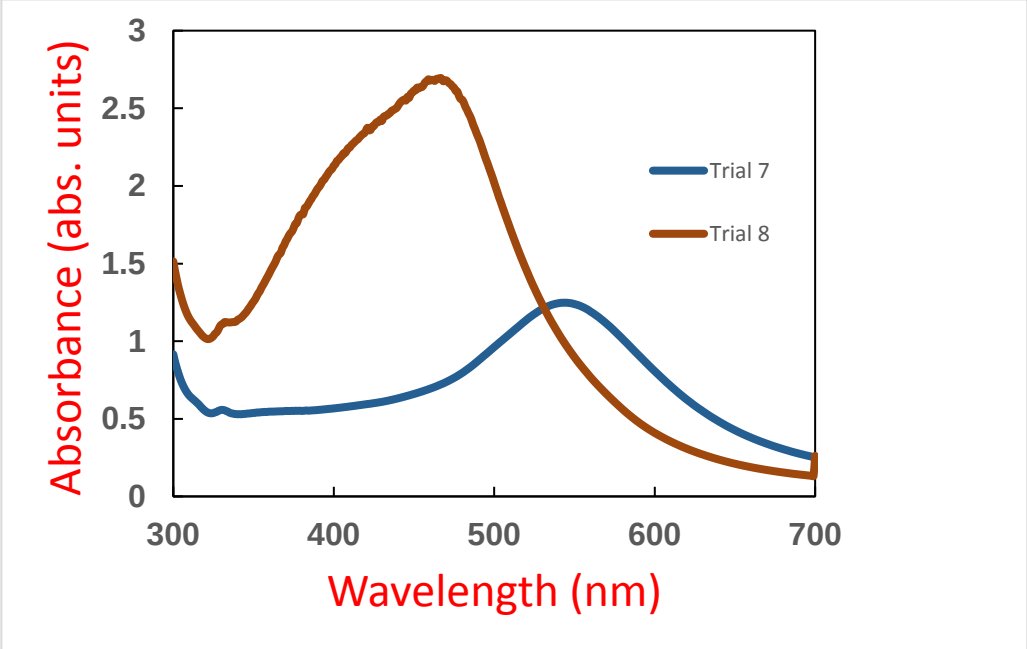

Figure 4.2: The UV-Vis absorbance peak for samples in trial 7 and trial 8.

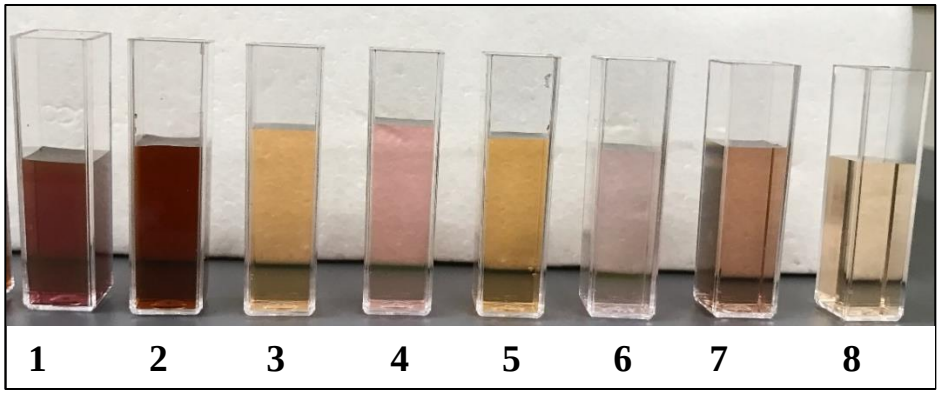

Figure 5: Photograph of cuvettes showing color differences in the samples of Ag nanoparticles prepared in trial 1 to trial 8.

Table 2 shows the amount of materials used in the preparation of large samples of Ag nanoparticles. The samples of trial 1 and trial 2 were analyzed using UV-Vis spectrophotometer to study their optical properties. The trial 1 was found to have λ_{max} at 480 nm whereas trial 2 was found to have a λ_{max} at 484 nm, because of the λ_{max} value and the sharpness of the peak obtained for trial 1 these solutions were used as a better option to carry out further reaction manipulations. The Ag nanoparticles obtained from the preparation using the trial 2 volumes of (Table 2) were used for the rest of the reactions to obtain Ag/Au, Ag/Pt and Ag/Pd nanoparticles.

Table 2: The amount of materials used in the preparation of large samples of Ag nanoparticles.

Trial #	Purified Water (mL)	10mM $AgNO_3$ (mL)	10mM Glutathione (mL)	0.1M NaOH (mL)	10mM $NaBH_4$ (mL)
1	50	3	0.3	10	3.6
2	50	0.7	0.1	10	3.6

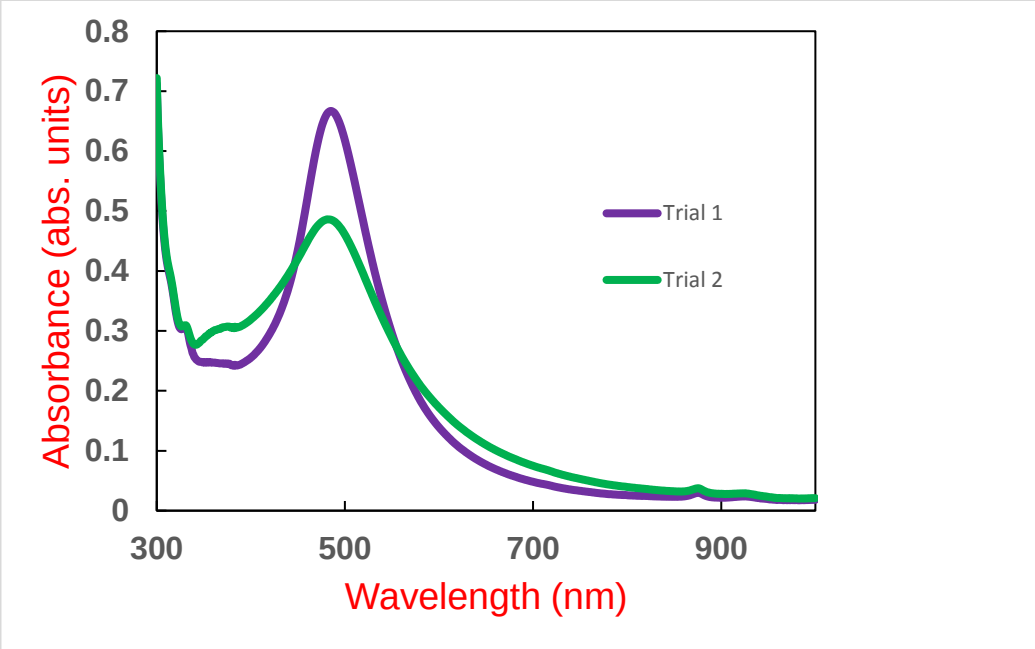

Figure 6: The UV-Vis absorbance peaks for samples trial 1 and trial 2 (Table 2) scanned from 1000 to 300 nm wavelength.

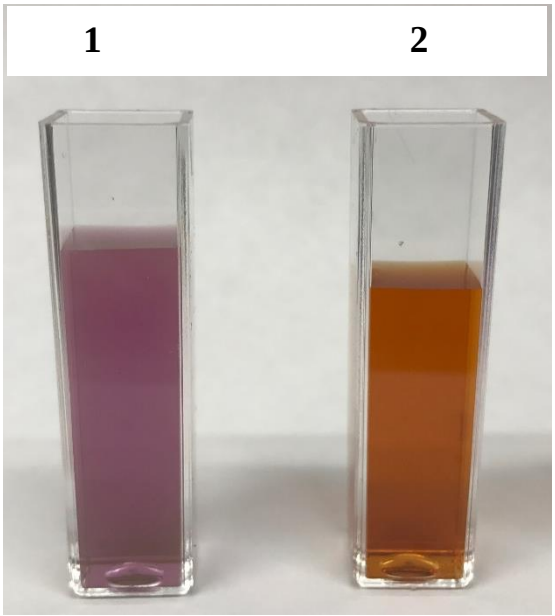

Figure 7: Photograph of cuvettes showing color difference in the samples of Ag nanoparticles prepared in large scale (trial 1 to trial 2).

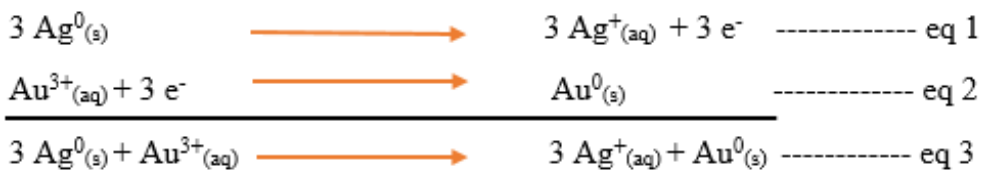

Because of the higher [28]standard potential of Au^{+3}/Au (1.50) compared to that of Ag^{+}/Ag (0.80), silver gets oxidized to silver ions and gold ions gets reduced to gold metal as shown in equation 3. For the synthesis of Au/Ag alloy we used $HAuCl_4$. Based on the stoichiometric relationship given below (equation 4) it is possible to convert silver metal into soluble species (Ag^{+}) while leaving behind a pure product of gold.

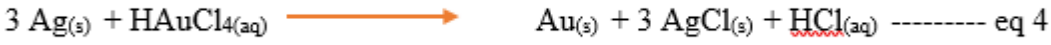

Since our research work was focused to form Au/Ag alloy, it was required to minimize the oxidation of the Ag so that enough Ag is still present during the reaction to play a role in template growth. For this requirement, we pursued a strategy in which measures were taken to maintain a sufficiently high level of the ascorbic acid as a reducing agent in the reaction mixture to provide substantial protection for the Ag hollow particle against complete oxidation during the galvanic replacement reaction. The reducing agent we used for this purpose was ascorbic acid. Due to the presence of excess of ascorbic acid, it is reasonable to expect that after initial oxidation of Ag from the Ag hollow particles by galvanic replacement, there is co-reduction of Ag^{+} and $AuCl_4^{-}$ to form Au/Ag alloy. Had we used an optimum amount of ascorbic acid, the co-reduction of Ag^{+} with $AuCl_4^{-}$ by ascorbic acid, it could have served to keep the concentration of Ag^{+} low enough to limit the formation of AgCl.

Transmission scanning electron microscopy (TEM) was employed to study the morphology of the Au/Ag, Pd/Ag, and Pt/Ag nanoparticles. Transmission electron microscopy (TEM) is a technique that utilized a beam of electrons that is transmitted through extremely small and thin specimens in a sample. The beam of electrons interacts with the specimens and image is formed from that interaction. Figure 8A shows the TEM images obtained for the Ag hollow nanoparticles produced by using a sample preparation obtained from trial 2 (Table 2) and Figure 8 B represents the TEM image of Ag/Au nanoparticles. The dark contrast areas in figure represents the multilayers of nanoparticles showing the 3-dimensional connectivity of nanoscale. The average particle size of the Ag hollow nanoparticles was found to be 65.0±9.0 nm whereas it was reduced to an average particle size of 7.0±1.6 nm for Ag/Au nanoparticles. The addition of 0.5 mM $HAuCl_4$ causes a reaction between the Ag hollow nanoparticles and the Au ion present in the salt solution, due to the reaction the Ag hollow nanoparticles tends to break into several nanoparticles and the broken parts of the nanoparticles are further surrounded by a layer of Au atoms to form a Ag/Au nanoparticles.

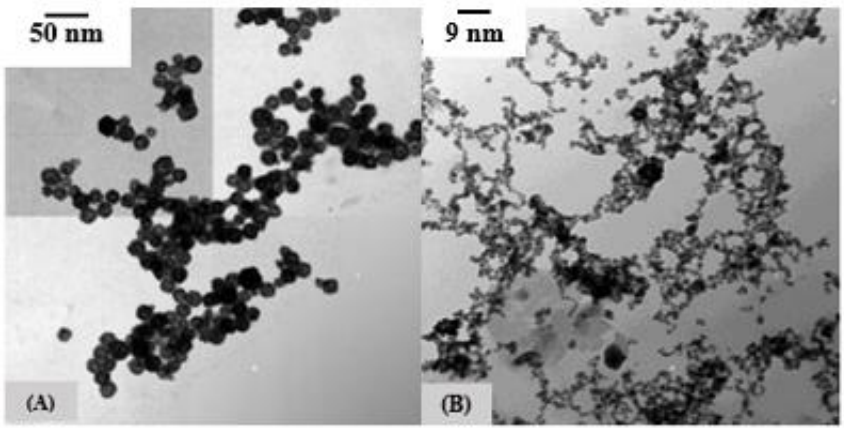

Figure 8: TEM images of the individual (A) Ag hollow nanoparticles, (B) Ag/Au alloy nanoparticles. The dark contrast areas represent the multilayers of nanoparticles showing 3-dimensional connectivity of nanoscale.

There is a chance of Ag ions to be formed in the process of reaction but they are removed as AgCl from the reaction such that all the nanoparticles thus formed will be of Ag/Au nanoparticles as a result of the reaction between Ag and $HAuCl_4$.

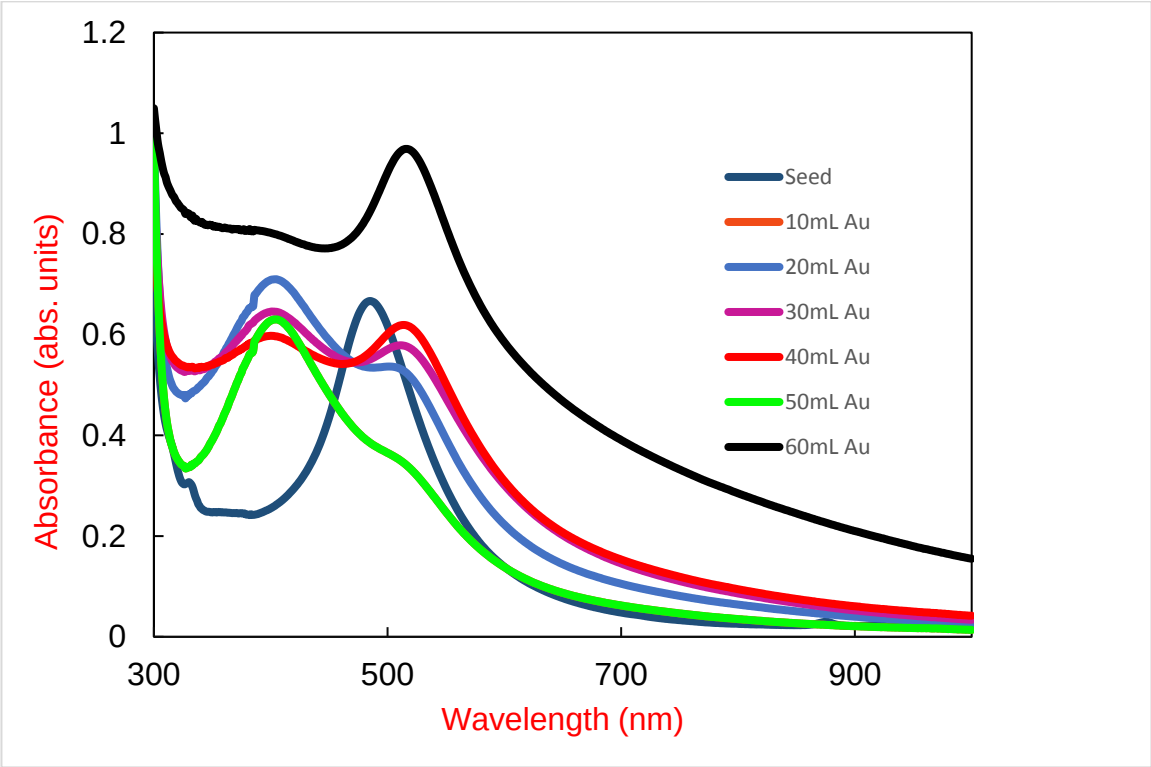

Figure 9: The UV-Visible absorption spectra of the Ag hollow particle solution obtained from trial 2 and series of Au/Ag samples obtained after addition of 10, 20, 30, 40, 50 and 60 mL of $HAuCl_4$ (0.5 mM).

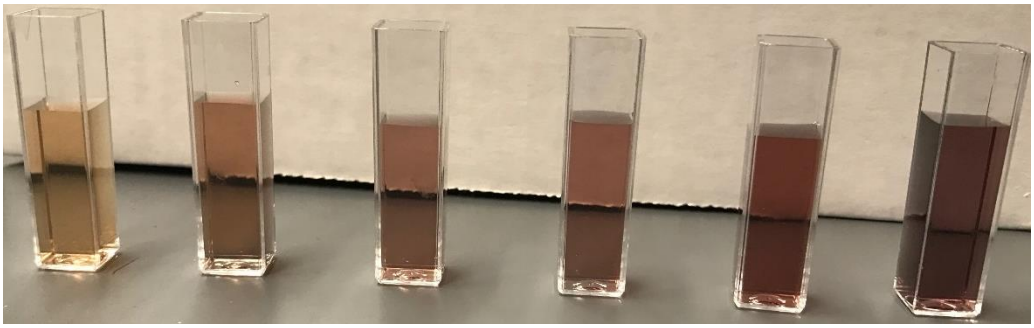

Figure 10: Photograph of cuvettes showing color differences in the samples after addition of 10, 20, 30, 40, 50 and 60 mL of $HAuCl_4$, respectively from left to right.

The reaction between Ag nanoparticles and $HAuCl_4$ showed a blue shift upon addition of 10 mL and 20 mL of 0.5 mM $HAuCl_4$ solution. The wavelength sifted from 490 nm to 414, 412, 409, 409 and 409 nm upon addition of 10, 20, 30, 40, and 50 mL of $HAuCl_4$ solution. Additional peaks were observed after the addition of 30 and 40 mL of $HAuCl_4$ solution. The wavelength after addition of all the 60 mL of $HAuCl_4$ solution showed only red shift and the peak was obtained at 518 nm. The extinction peak corresponding to Ag nanoparticles (at 490 nm) disappeared and additional peak showing a red shift was formed when 30 mL of $HAuCl_4$ solution was introduced into the reaction system. This change indicated the consumption of templates made of pure Ag and the formation of nanoparticles made of a homogeneous Ag/Au alloy. Accompanying the formation of Au/Ag nanoparticles, an extinction peak with increasing intensity appeared at longer wavelengths, whose position was continuously red-shifted towards 525 nm.

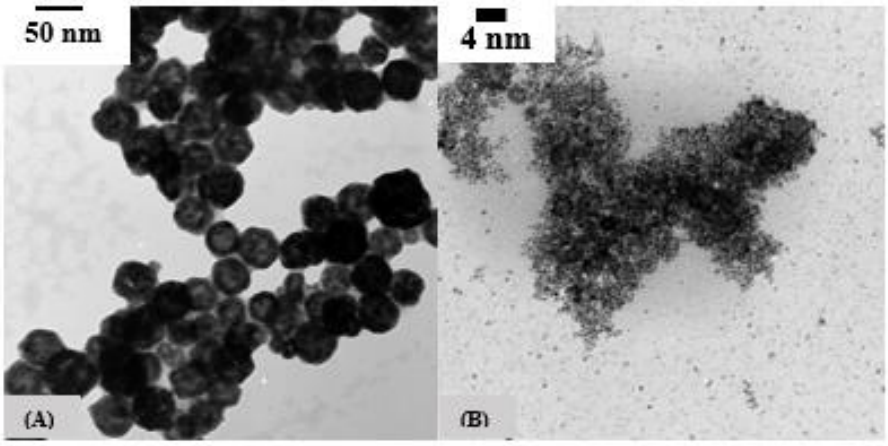

Figure 11: TEM images of the individual (A) Ag hollow nanoparticles, (B) Ag/Pd alloy nanoparticles. The dark contrast areas represent the multilayers of Nanoparticles showing 3-dimensional connectivity of nanoscale.

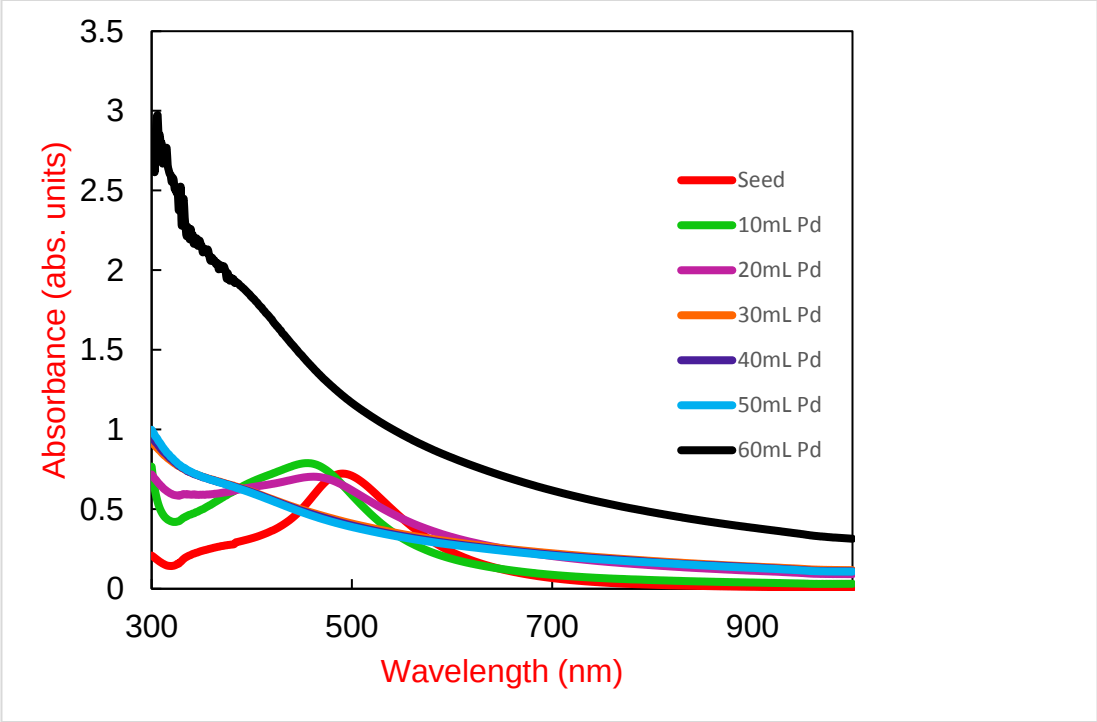

Figure 12: UV-Visible absorption spectra of the Ag seed solution and series of Pd/Ag samples obtained after addition of 10, 20, 30, 40, 50 and 60 mL of K_2PdCl_4 (0.5 mM).

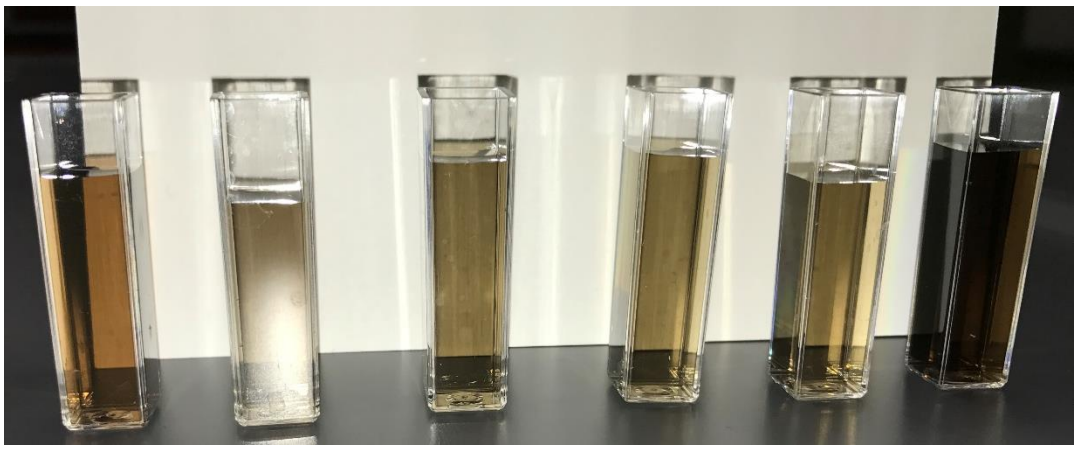

Figure 13: Photograph of cuvettes showing color differences in the samples after addition of 10, 20, 30, 40, 50 and 60 mL of K_2PdCl_4, respectively from left to right.

TEM images of the individual Ag hollow nanoparticles were shown in Figure 11A and Ag/Pd nanoparticles were shown in Figure 11 B. The average particle size of the Ag nanoparticles was found to be 65.0±9.0 nm. The particle size in the reaction containing K_2PdCl_4 was greatly reduced when compared to that of the reaction containing Au salt. The average particle size of the Ag/Pd hollow nanoparticles was found to be 6.0±1.2nm. The reduction in the particle size is due to the change the metal ion being used to break the Ag hollow nanoparticles. Figure 12 shows the UV-Visible absorption spectra of the Ag seed solution and series of Pd/Ag samples obtained after addition of 10, 20, 30, 40, 50 and 60 mL of K_2PdCl_4 (0.5 mM). The addition 10 mL of K_2PdCl_4 shifted the wavelength towards the blue shift and the peak was completely disappeared after addition of 30 mL of the Pd salt solution. A flat spectrum was obtained after addition of the whole 60 mL solution containing 0.5 mM K_2PdCl_4.

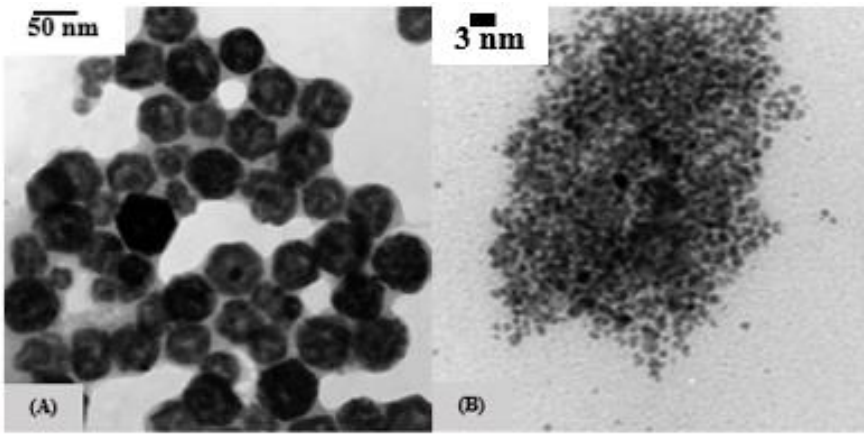

Figure 14: TEM images of the individual (A) Ag hollow nanoparticles, (B) Ag/Pt Nanoparticles.

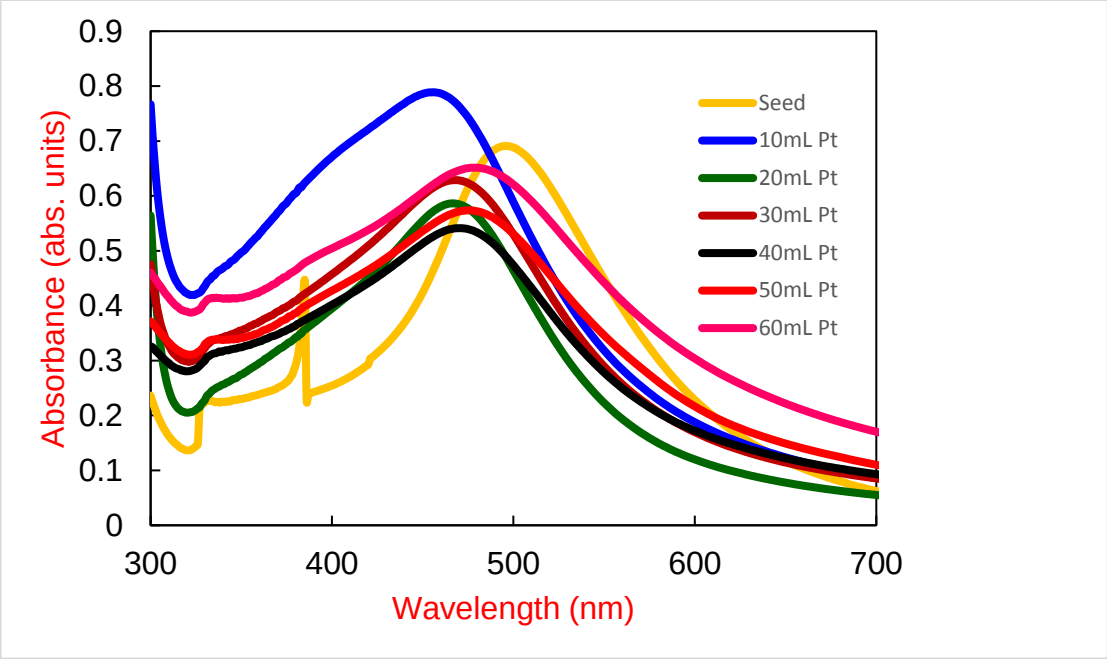

Figure 15: UV-Visible absorption spectra of the Ag seed solution and series of Pt/Ag samples obtained after addition of 10, 20, 30, 40, 50 and 60 mL amounts of K_2PtCl_4 (0.5 mM).

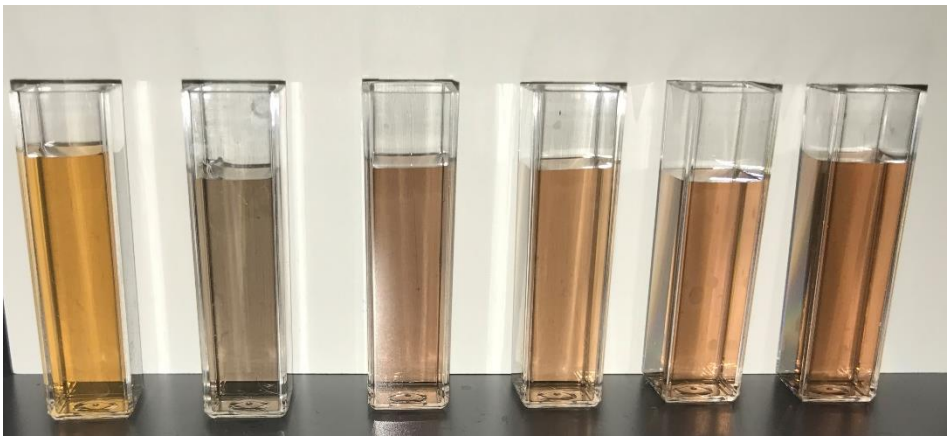

Figure 16: Photograph of cuvettes showing color differences in the samples after addition of 10, 20, 30, 40, 50 and 60 mL of K_2PtCl_4, respectively from left to right.

The TEM images obtained after the reaction of K_2PtCl_4 with Ag nanoparticles were shown in Figure 14. The average particle size of the Ag nanoparticles was 65.0±9.0 nm whereas the average particle size of the Ag/Pt nanoparticles was found to be 3.0±0.8 nm which is almost half the size of the Ag/Au hollow nanoparticles. In Figure 14 A the TEM image of the Ag hollow nanoparticles were shown and in Figure 14 B Ag/Pt nanoparticles is shown. Figure 15 shows the UV-Visible absorption spectra of the Ag seed solution and series of Pt/Ag samples obtained after addition of 10, 20, 30, 40, 50 and 60 mL amounts of K_2PtCl_4 (0.5 mM). The wavelength showed a blue shift by decreasing the wavelength from 490 nm to 461 nm after the addition of 10 mL of K_2PtCl_4 (0.5 mM) solution. The blue shift continued up to 30 mL addition of K_2PtCl_4 (0.5 mM) solution, there was a red shift upon addition of 40 mL of Pt salt solution from 459 to 474 nm. The red shift continued until the final addition of the Pt salt solution and the wavelengths of 474 nm, 481nm and 484 nm were obtained for the samples analyzed after addition of 40, 50 and 60 mL of K_2PtCl_4 (0.5 mM) solution, respectively. Retaining the peak after addition of all the solution of K_2PtCl_4 shows that the Ag/Pt reaction was successfully carried out.

Powder X-Ray Diffraction (PXRD) is a technique that uses X-ray diffraction on microcrystalline samples for structural characterization of materials. The powder samples were deposited on a glass slide for XRD measurements. X-ray diffraction patterns were identified by comparing them to the phases in X'Pert Highscore Plus along with the ICDD/JCPDS diffraction pattern library. An advantage of X-ray diffraction is that this method provides a very simple possibility for estimating the particle size from the broadening of the XRD reflections by means of the Scherrer formula.

$$d = K\lambda/\omega \cos\Theta$$

Where d is the particle size, λ is the wavelength of the radiation, θ is the angle of the considered Bragg reflection, ω is the width on a 2θ scale, and K is a constant close to unity.

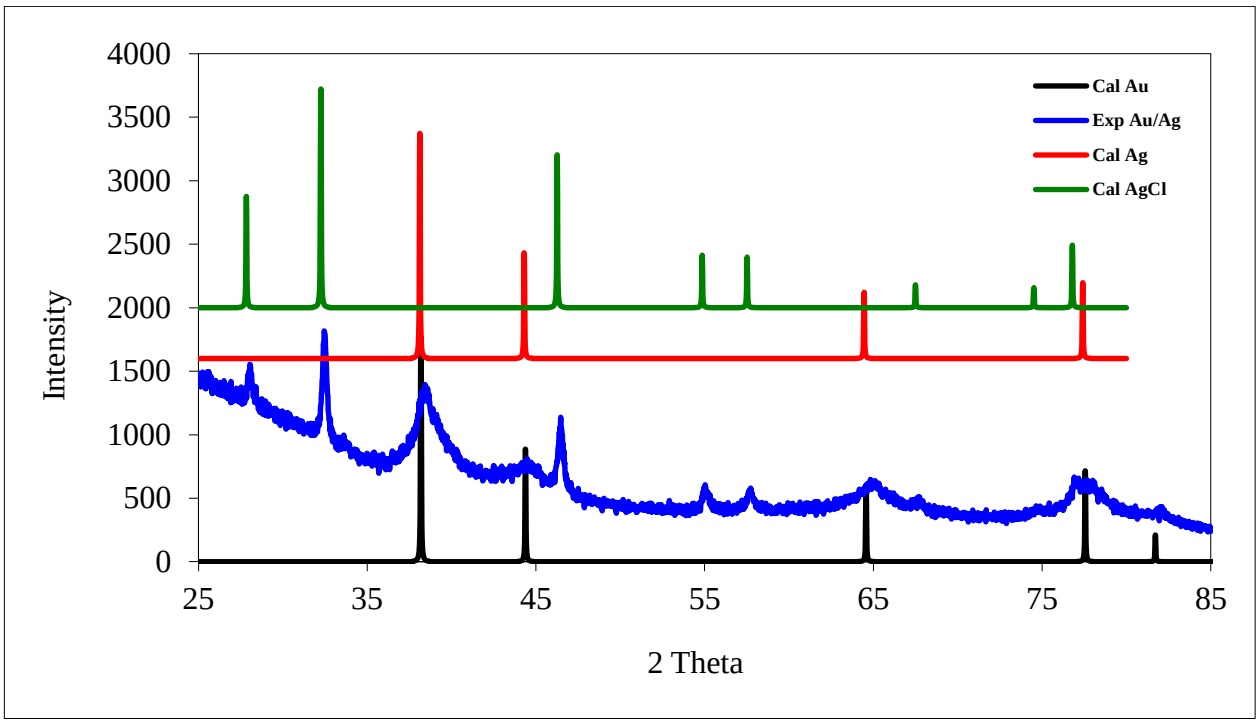

Figure 17: PXRD patterns of Au/Ag particles.

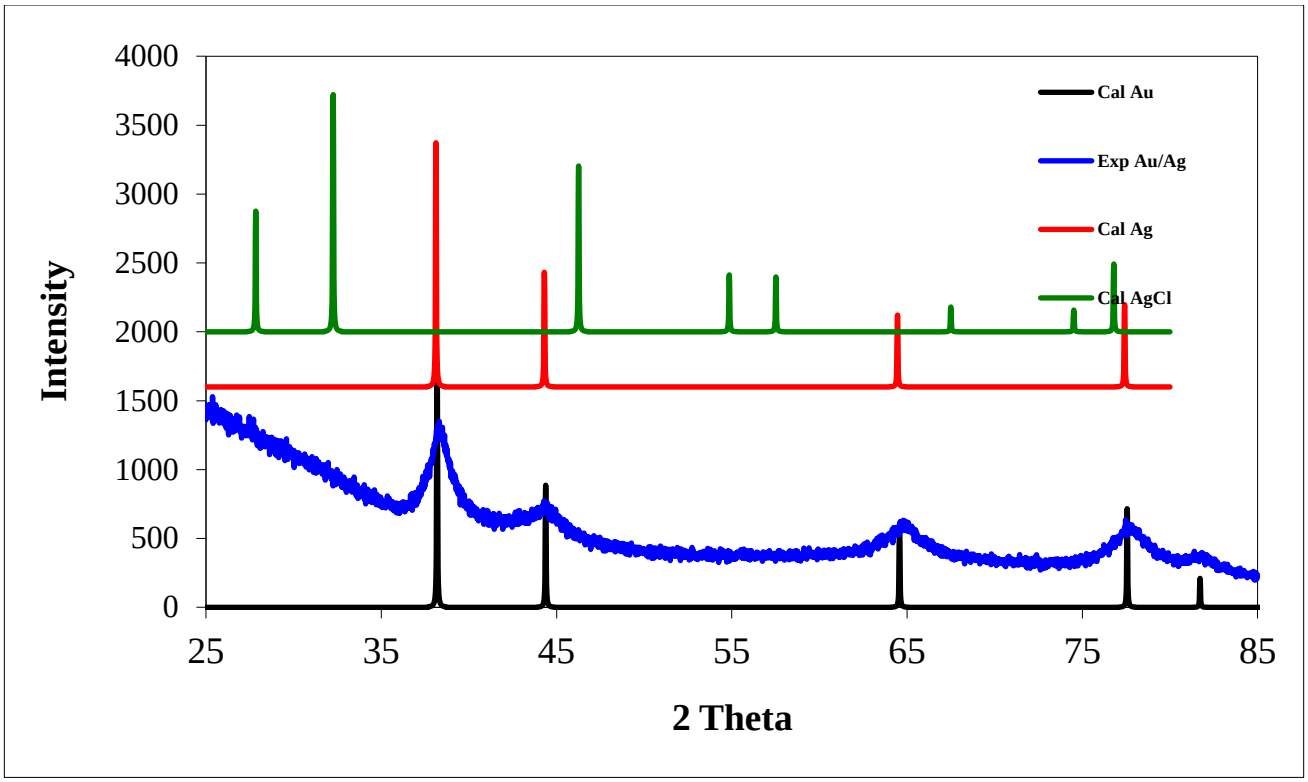

Figure 18: PXRD patterns of Au/Ag particles washed with NH_3.

The PXRD crystallogram contains the data for calculated Au and for the experimental Ag/Au sample. The slight shift of the powder pattern toward smaller 2θ angles indicates the growth of bimetallic Ag/Au hollow nanoparticles. Figure 17 indicates the PXRD patterns for calculated Au, experimental Au/Ag sample, calculated Ag, and calculated AgCl. Figure 18 inicates the PXRD patterns of calculated Au, experimental Au/Ag washed with NH_3, calculated Ag and calculated AgCl. The small peaks are attributed to AgCl which was formed during the reaction. It can be noticed that the smaller peaks corresponding to AgCl in the experimental pattern are not present after sample is washed with NH_3. The most intense peak for the experimental Ag/Pd after being washed with NH_3 falls between the most intense peaks for calculated Ag and calculated Au, this verifies the synthesis of bimetallic Au/Ag. The average particle calculated by using the Scherrer formula was found to be 3.25 nm which was

found to be a close value obtained from TEM image. In order to understand the PXRD of the alloy nanoparticles, the pure Ag sample is being prepared and the data of experimental pure Ag will be incorporated into the provided PXRD.

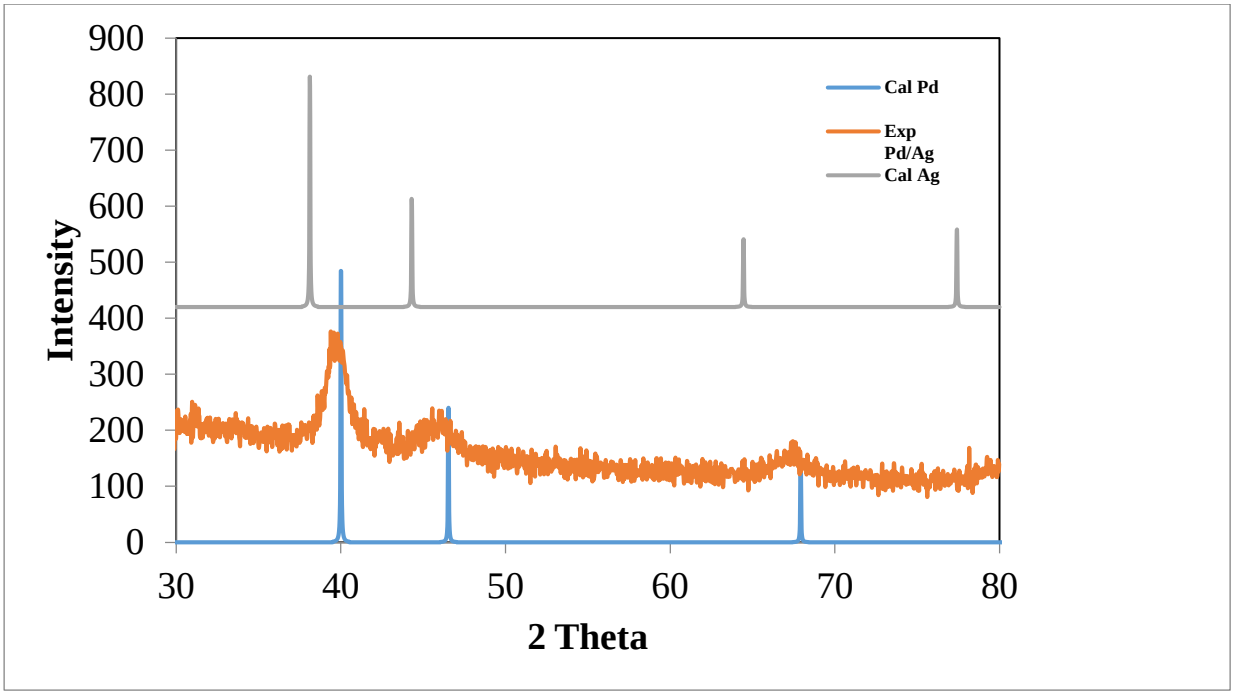

Figure 19: PXRD patterns of Pd/Ag particles.

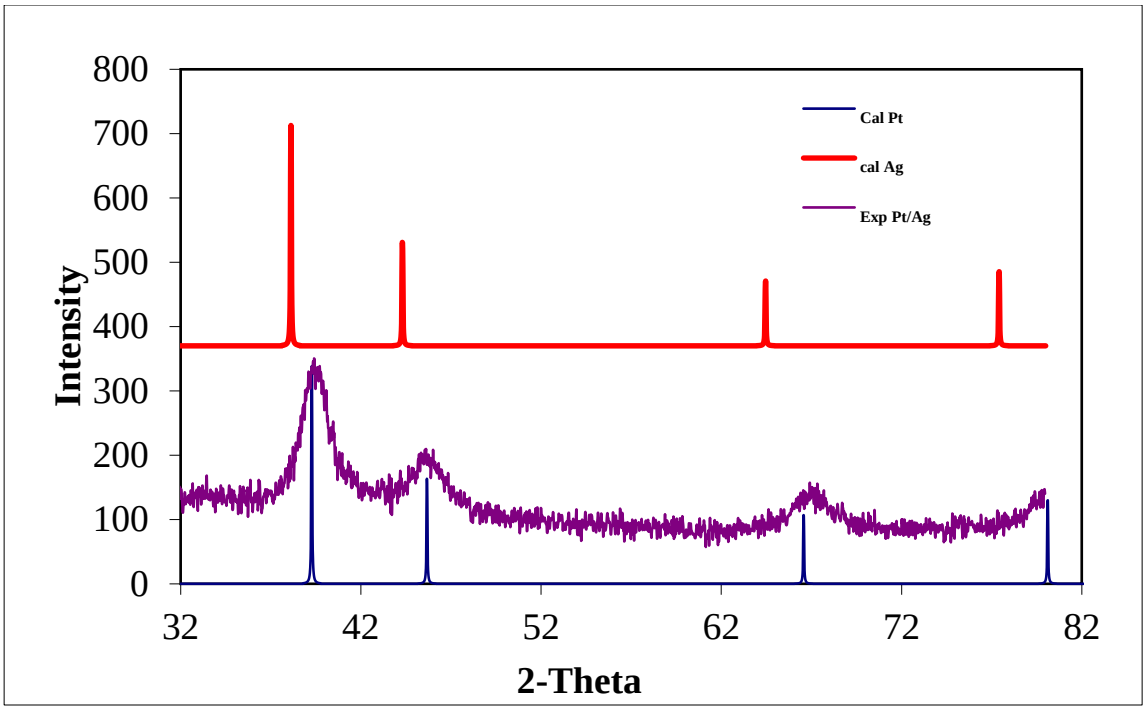

Figure 20: PXRD patterns of Pt/Ag particles.

Figure 19 shows the PXRD patterns containing calculated Pd, experimental Pd/Ag sample and calculated Ag. In Pd/Ag Nanoparticles the intense peaks were observed in the range of 35 to 50, 2θ values. The average particle size was found to be 3.41 nm for Pd/Ag hollow Nanoparticles using Scherrer formula. In Figure 20 the PXRD patterns of calculated Pt, experimental Pt/Ag sample and calculated Ag are shown. Using Scherrer formula Pt/Ag hollow Nanoparticles average particle size was found to be 2.84 nm which was close to the value of 3.04 obtained from the TEM images.

Conclusion

In conclusion, a new approach for the controllable synthesis of Au/Ag, Pd/Ag, and Pt/Ag alloy nanoparticles by applying galvanic replacement reaction on hollow Ag template in the presence of gold, palladium, and platinum salts was successfully investigated. The bimetallic nanoparticles were studied using UV-Vis, TEM, and PXRD. The addition of varying amounts K_2PdCl_4 and K_2PtCl_4 showed a diminish in the surface plasmon peaks, but interestingly our attempt to make Pt/Ag particle by reacting Ag hollow particles with various amounts of K_2PtCl_4 revealed that resulting alloy particles could still exhibit surface plasmon resonance peaks for higher Pt content. This work provides a model for a design of M/Ag; M=Au, Pt, Pd alloy particles, where combining Ag hollow samples with increasing amounts of Au, Pt, and Pd can provide successful execution of tenability of surface plasmon resonance.

References

1. Satoshi, H.; Nick, S.; *Microwaves in Nanoparticle Synthesis, First Edition; Wiley online library*; **2013**; 10.1002/9783527648122.ch1 (accessed 04/05/2017)
2. Aherne, D. Gara, M.; Kelly, J. M.; Gun'ko, Y. K. *Adv. Funct. Mater.* **2010**, *20*, 1329–1338
3. Zaleska-Medynska, A.; Marchelek, M.; Diak, M.; Grabowska E. *Adv. Colloid Interface Sci.* **2016**, *229*, 80–107.
4. Xia, Y.; Halas, N.J. *MRS Bull.* **2005**, *30*, 338-348.
5. Schulz, J.; Roucoux, A.; Patin, H. *Chem. Rev.* **2002**, *102*, 3757-3778.
6. Toshima, N.; Yonezawa, T. *New J. Chem.* **1998**, *11*, 1179-1201.
7. Sun, S.; Murray, C.B.; Weller, D.; Folks, L; Moser, A. *Science* **2000**, *287*, 1989-1992.
8. Sun, Y.; Xia, Y. *J. Am. Chem. Soc.* **2004**, *126*, 3892-3901.
9. Creighton, J.A.; Eadon, D.G. *J. Chem. Soc. Faraday Trans.* **1991**, *87*, 3881-3891.
10. Xiong, Y.; Wiley, B.; Chen, J.; Li, Z.; Yin, Y.; Xia, Y. *Angew. Chem. Int. Ed.* **2005**, *44*, 7913-7917.
11. Yadong, Y.; Robert, M. R.; Can, K. E.; Steven, H.; Gabor, A. S.; Paul, A. *Science* **2004**, *304*, 711-714.
12. Jin, F. H.; Ulrich, G.; Margit, Z. *Small* **2007**, *3(10)*, 1660-1671.
13. Smigelskas, A. D.; Kirkendall, E. O. *Trans. AIME* **1947**, *171*, 130-142.
14. Sun, Y.; Mayers, B. T.; Xia, Y. *Nano Lett.* **2002**, *2*, 481−485.
15. Xia, X.; Wang, Y.; Ruditskiy, A.; Xia, Y. *Adv. Mater.* **2013**, *25*, 6313−6333.
16. Liu, Y.; Goebl, J.; Yin, Y. *Chem. Soc. Rev.* **2013**, *42*, 2610−2653.
17. Zhang, H.; Jin, M.; Liu, H.; Wang, J.; Kim, M. J.; Yang, D.; Xie, Z.; Liu, J.; Xia, Y. *ACS Nano* **2011**, *5*, 8212−8222.

18. Alia, S. M.; Yan, Y. S.; Pivovar, B. S. *Catal. Sci. Technol* **2014**, *4*, 3589−3600.

19. Gilroy, K. D.; Farzinpour, P.; Sundar, A.; Hughes, R. A.; Neretina, S. *Chem. Mater.* **2014**, *26*, 3340−3347.

20. Song, H. M.; Anjum, D. H.; Sougrat, R.; Hedhili, M. N.; Khashab, N. M. *J. Mater. Chem.* **2012**, *22*, 25003−25010.

21. Wang, C.; Wang, Y.; Xu, L.; Shi, X.; Li, X.; Xu, X.; Sun, H.; Yang, B.; Lin, Q. A. *Small* **2013**, *9*, 413−420.

22. Lu, X.; Au, L.; McLellan, J.; Li, Z.-Y.; Marquez, M.; Xia, Y. *Nano Lett.* **2007**, *7*, 1764−1769.

23. Chen, Z.; Waje, M.; Li, W.; Yan, Y. *Angew. Chem Int. Ed.* **2007**, *46*, 4060−4063.

24. Wan, D.; Xia, X.; Wang, Y.; Xia, Y. *Small* **2013**, *9*, 3111−3117.

25. Zhang, G.; Sun, S.; Cai, M.; Zhang, Y.; Li, R.; Sun, X. *Sci. Rep.* **2013**, *3*, 1526-1533.

26. Moshe, A. B.; Markovich, G. *Chem. of Mater.* **2011,** *23 (5)*, 1239-1245.

27. Borchert, H.; Shevchenko, V.; Robert, A.; Mekis, I.; Kornowski, A.; Grubel, G.; Weller, H. *Langmuir* **2005**, *21*, 1931-1936.

28. Milazzo, G.; Caroli, S.; Sharma, V. K.; Wiley J. *Tables of standard electrode potentials* **1991**, 1, 5-80.